Hindawi Publishing Corporation
Journal of Thermodynamics
Volume 2010, Article ID 452326, 13 pages
doi:10.1155/2010/452326

Research Article

Laboratory-Scale Experiments of the Methane Hydrate Dissociation Process in a Porous Media and Numerical Study for the Estimation of Permeability in Methane Hydrate Reservoir

Yasuhide Sakamoto,[1] Takeshi Komai,[1] Kuniyuki Miyazaki,[1] Norio Tenma,[1] Tsutomu Yamaguchi,[2] and George Zyvoloski[3]

[1] *National Institute of Advanced Industrial Science and Technology (AIST), Tsukuba, Ibaraki 305-8568, Japan*
[2] *Department of Environmental Science, Faculty of Science, Toho University, Funabashi, Chiba 134-8540, Japan*
[3] *Earth and Environmental Science Division, Los Alamos National Laboratory (LANL), Los Alamos, NM 87545, USA*

Correspondence should be addressed to Yasuhide Sakamoto, sakamoto-yasuhide@aist.go.jp

Received 3 August 2009; Accepted 1 December 2009

Academic Editor: Costas Tsouris

Copyright © 2010 Yasuhide Sakamoto et al. This is an open access article distributed under the Creative Commons Attribution License, which permits unrestricted use, distribution, and reproduction in any medium, provided the original work is properly cited.

An experimental study of the dissociation of methane hydrate (MH) by hot-water injection and depressurization was carried out at the National Institute of Advanced Industrial Science and Technology (AIST). These experiments helped us understand some important aspects of MH behavior such as how temperature, pressure, and permeability change during dissociation and gas production. In order to understand the experimental results, a model of MH dissociation in a porous media was designed and implemented in a numerical simulator. In the model, we treated the MH phase as a two-component system by representing the pore space occupied by MH as a separate component. Absolute permeability and relative permeability were formulated as a function of MH saturation, porosity, and sand grain diameter and introduced into the numerical model. Using the developed numerical simulator, we attempted history matching of laboratory-scale experiments of the MH dissociation process. It was found that numerical simulator was able to reproduce temperature change, permeability characteristics, and gas production behavior associated with both MH formation and dissociation.

1. Introduction

Methane hydrate (MH) is an ice-like solid substance in which a water molecule structure contains embedded methane molecules under low-temperature and high-pressure conditions. When 1 m^3 of MH is decomposed, approximately 150 m^3 of methane gas is produced at standard conditions. In the near future, MH will be a potential resource of natural gas, because vast amounts of MH reservoirs exist in marine sediments and in permafrost regions worldwide [1–5] .

Some extraction methods of MH from reservoirs in marine sediments have been proposed, such as depressurization, thermal stimulation, and inhibitor injection (Makogon, 1981). All are based on the in-situ dissociation of MH that is transformed into methane gas and water. It is likely that this process consists of the following physical phenomena .

(1) The porosity and permeability of porous media are changed as a result of MH dissociation.

(2) Dissociated gas and water migrate through pore space, which is enlarged by the dissociation of MH crystals that has functioned as a binder between sand grains.

(3) The temperature and enthalpy are changed by the generation of heat and mass flows due to MH dissociation.

All the proposed extraction methods have drawbacks. In the thermal stimulation process, the thermal efficiency for injected fluid is low. Temperature losses in the drill pipe and heat conduction in the host rock and sediments severely limit the heat available for dissociation. In the inhibitor injection process, chemical materials used as inhibitors are costly and

are of unproven value in marine environments. In addition, environmental risk due to utilization of such materials has not been evaluated. Therefore, depressurization process is regarded as the most effective process for gas recovery from the viewpoints of gas productivity, safety, and economical efficiency, compared with the other in-situ dissociation processes [6]. However, an increase in effective stress during depressurization can cause consolidation of MH sediments and permeability reduction [7]. As a result, reduction of gas productivity is likely over time with depressurization. Even though heat is not added during the depressurization process, the latent heat requirement for dissociation causes cooling and a reduction in dissociation rate. Therefore, it is very important to understand the behavior of an MH reservoir, especially during the extraction phase and when considering the environmental impacts due to reservoir operation .

In order to safely and efficiently design and operate an MH reservoir, it is necessary to develop a numerical simulator for prediction of gas productivity from an MH reservoir and carry out a parametric study for the optimization of gas production. Some numerical studies of MH dissociation in porous media have been reported. These studies are classified into (1) the analysis of the physical phenomena observed in laboratory-scale experiments, such as the movement of the MH dissociation front and the flow behavior of gas and water, and (2) field-scale simulations of a potential MH resource. Yousif et al. [8] developed a one-dimensional simulator for depressurization in Berea sandstone core and conducted an analysis of the MH saturation distribution and production behavior of gas and water and the movement of the dissociation front. Selim and Sloan [9] suggested a one-dimensional MH dissociation model for heat stimulation methods. They distinguished between the dissociated zone saturated with gas and water and the nondissociated zone and developed some analytical solutions. Jeannin et al. [10] investigated the dissolution of methane gas into the water phase and treated methane mole fraction in water as the driving force for dissociation in their simulation model. Holder and Angert [11] developed a three-dimensional simulator for depressurization intended for an MH reservoir located over a free-gas layer. Masuda et al. [12] developed a multidisciplinary field-scale simulator, including dissociation rate, endothermic reaction due to dissociation, mass flows and heat transfer and carried out a parameter study for the various gas extraction methods for an MH reservoir. Although the permeability of the MH reservoir is one of the most important parameters affecting the flow of gas and water during dissociation, and in predicting gas productivity, there is little research on the change in effective permeability with MH formation and dissociation. Therefore, it is necessary to develop a conceptual model for the change in permeability with MH formation and dissociation and implement this conceptual model into the numerical simulator.

We have performed laboratory-scale experiments on MH dissociation processes in porous media by hot-water injection and depressurization in order to understand several phenomena that occur during MH formation and dissociation. These include temperature and permeability changes, dissociation kinetics, and gas production behavior. On the basis of the experimental results, we constructed a numerical representation of MH dissociation in porous media. We also measured the absolute permeability and relative permeability with MH formation and formulated permeability as a function of MH saturation, porosity, and sand grain diameter. Using the developed numerical simulator, we attempted history matching of laboratory-scale experiments for MH dissociation process, validated the numerical model, and improved our understanding of the evolution of permeability during MH extraction.

2. Experimental Evaluation of Permeability Characteristics during MH Dissociation Process in Porous Media

Firstly, in order to understand permeability change and gas-water multiphase flow during MH dissociation process in porous media, we carried out an experimental study on hot-water injection as a way to enhance MH dissociation. In this study, we used several types of sand columns in which sand grains and water were packed into a high-pressure stainless steel vessel as model MH reservoirs. The internal diameter of the vessel is 65 mm, and the length is 539 mm. The experiment's pressure and temperature were limited to 15 MPa and 50°C, respectively. The vessel was set vertically, and the fluid was injected at the top edge and produced at the bottom edge of the vessel. On the basis of measured differential pressure between upper and lower edges of sand column, water effective permeability with MH formation was expressed as a multiplier of absolute permeability and relative gas, and liquid permeabilities were also calculated during MH dissociation. The details of the apparatus and experimental procedure have been published previously [13]. As an example of permeability change and gas production behavior during MH dissociation by hot-water injection, the results for injected water and dissociation pressure of 41°C and 10 MPa, respectively, are shown in Figure 1. The figure shows the changes in temperature distribution, differential pressure, water permeability, and production behavior of gas and water with time. From this figure, it was found that MH dissociation by hot-water injection consisted of four stages: (1) displacement of free methane gas due to water injection, (2) permeability reduction due to additional MH formation in the downstream zone, (3) MH dissociation due to hot-water injection, and (4) completion of the dissociation. In particular, the MH reformation and growth observed at the initial stage had large effect on the dissociation behavior and permeability characteristics. We also carried out an experimental study of the simultaneous injection process of nitrogen and hotwater [14] (Sakamoto et al., 2005). Nitrogen acts as an inhibitor; methanol and salts are other well-known inhibitors. The same apparatus used for the hot water injection was also used to simultaneously inject nitrogen and hot-water. This was done to evaluate the mixtures ability to prevent permeability reduction due to MH reformation and growth and to promote additional MH dissociation. The

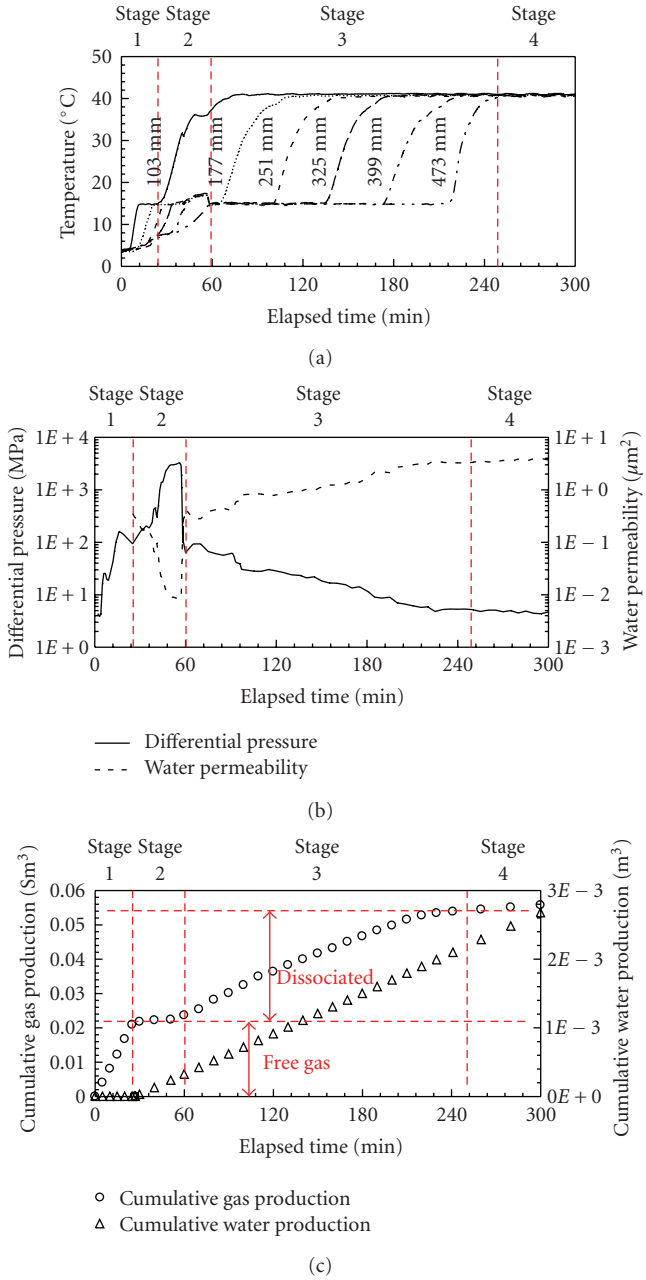

Figure 1: Temperature and water permeability in sand column and gas production behavior in MH dissociation by hot-water injection: (a) temperature, (b) differential pressure and water permeability, and (c) cumulative production of gas and water.

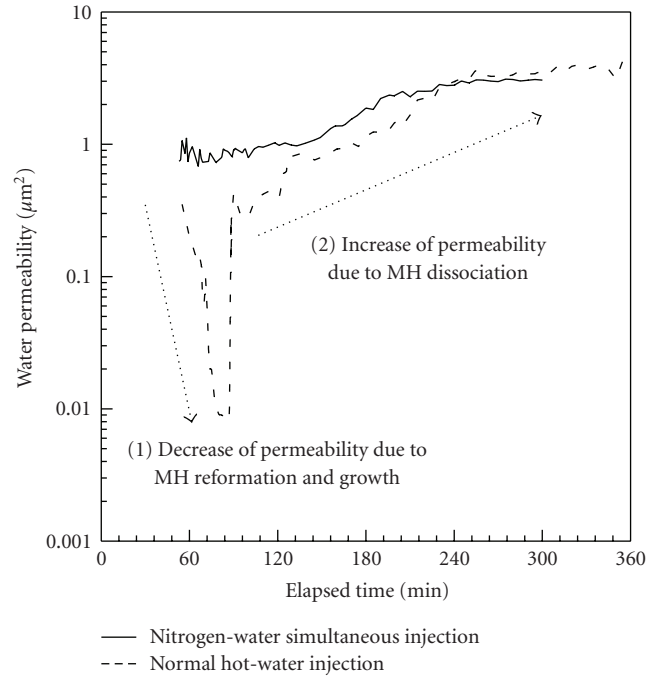

Figure 2: Change of water permeability with time in the cases of nitrogen-water simultaneous injection and normal hot-water injection.

nitrogen mixture is effective because the mole fraction of methane in the gas phase is reduced by injecting nitrogen and the equilibrium condition of MH is shifted to a lower temperature and higher pressure. Figure 2 shows the changes of water permeability with time during nitrogen-hot-water simultaneous injection process. For comparison, the result of normal hot-water injection process as shown in Figure 1 was also plotted in Figure 2. As previously mentioned, permeability was significantly decreased due to MH reformation and growth in downstream zone of sand column at the early times with (only) hot-water injection. On the other hand, only a small permeability decrease with a gradual recovery was observed during the simultaneous injection process. In this experiment, MH is formed in the pore space by injecting high-pressure methane gas into the sand column under the condition of irreducible water saturation. Silica sand shows the tendency to water wet, so MH that existed before injection is treated as that formed on the surface of the sand grains. This MH derived from irreducible water decreases the effective flow path in the pore space depending on the irreducible water saturation. In this case, the permeability in a reservoir decreases gradually as MH saturation becomes higher, but plugging of pore space does not occur [15]. Therefore, it is probable that this significant permeability decrease observed in the case of only hot-water injection was due to the movement of dissociated gas and movable (injected) water reacting to reform MH in the pore space . This movable water is defined as "free water" as opposed to "irreducible water."

We also conducted laboratory-scale depressurization experiments to study permeability change due to reservoir consolidation. This is important because we expect some porosity change (and related permeability change) from mechanical compaction as result of MH dissociation and gas production. In order to develop models of porosity and permeability changes as a result of MH dissociation, pore changes from compaction must also be evaluated. A special type of apparatus was used to evaluate the horizontal permeability characteristics associated with vertical consolidation. The details of the apparatus and experimental procedure have been published in a previous paper [16]. The testing

cell consisted of a stainless steel ring (internal diameter: 150 mm, wall thickness: 100 mm, and maximum pressure: 15 MPa) and upper and bottom plates for pressurization. In order to simulate MH sediments, we used several types of sands. An axial load that simulated rock stress conditions in marine sediments was applied on the upper edge of the sand pack using a loading piston. In order to initiate MH dissociation, the pore pressure was decreased at the center of the sand pack with a back-pressure regulator. Dissociation pressure and initial total stress by axial loading were set to 3 MPa and 11 MPa, respectively. We used the following two conditions to evaluate consolidation behavior due to the change in effective stress. In Run No.1, pore pressure decreased from 10 to 3 MPa while maintaining an axial load of 11 MPa. In this case, effective stress increased from 1 to 8 MPa with depressurization. On the other hand, the effective stress during MH dissociation in Run No.2 was maintained at 1 MPa in spite of the pore pressure change. Figure 3 shows the dependence of effective stress on the consolidation behavior during depressurization. When the effective stress reached 8 MPa with depressurization, marked consolidation occurred in Run No.1. Then, consolidation gradually proceeded. The compressive strain, which is the amount of consolidation divided by the initial height of the sand pack, ultimately reached 1.47×10^{-2}. However, the strain after 2 minutes was 0.97×10^{-2}. Therefore, at the initial stage in which the effective stress was increased, the amount of consolidation was approximately 65.7% of the final value. On the other hand, the compressive strain in Run No.2 was maintained at a small value as the MH dissociation proceeded. From these results, we concluded that the volumetric change in the solid material due to MH dissociation was small. Therefore, the increase in the effective stress is a dominant factor for the consolidation behavior, and most of the consolidation occurs at the initial stage of depressurization. It is particularly important to predict permeability change at this stage, because of dissociated gas and water flow into the region where MH dissociation has already occurred. Therefore we estimated the effect of porosity reduction due to consolidation on permeability independently from changes of MH dissociation and formation.

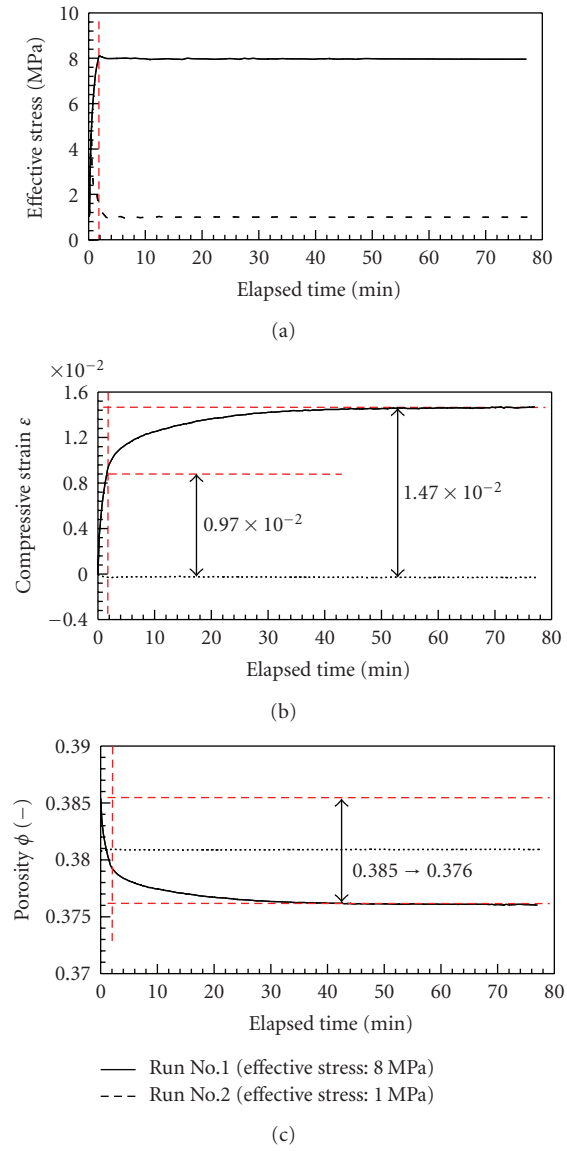

Figure 3: Consolidation behavior during MH dissociation in different effective stress case.

3. Development of Numerical Model for MH Dissociation Process in a Porous Media and Experimental Estimation of Permeability with MH Formation

3.1. Modeling Pore Space Occupied by MH. To develop a numerical model for MH dissociation process in porous media, it is necessary to model the pore space occupied by of MH. On the basis of observations of permeability characteristics in the laboratory studies, we defined two components of MH in pore space. Figure 4 shows the conceptual model of MH phase that exists in the pore space. One MH component (S_{h1}) is derived from irreducible water. This is formed as a cover on the surface of a sand grain, and it is assumed that the effect on the permeability characteristics is small. This MH component exists under the initial experimental conditions. The other MH component (S_{h2}) is derived from moveable free water. The MH derived from free water is formed inside the pore space and generally plugs the flow path. It has a marked effect on permeability as observed in the experiments. In our conceptual model, the MH growth or formation rate is associated only with MH saturation S_{h2} derived from free water. The MH saturation S_{h1} derived from irreducible water does not change with time when temperature and pressure conditions are such that MH should form. In addition, we assume that the dissociation of MH derived from free water is preferentially started, because this MH exists in the neighborhood of a flow path and the heat available from injected water is preferentially supplied to this component.

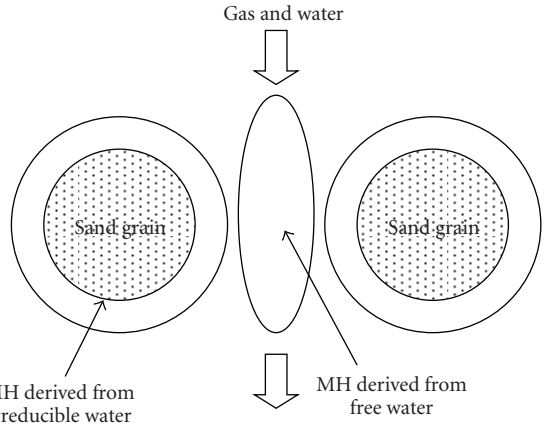

Figure 4: Schematic of MH two-component system.

The numerical model consists of a three-phase four-component system: gas, water, MH derived from irreducible water, and MH derived from free water.

3.2. Governing Equation in Porous Media with MH Formation

3.2.1. Mass Conservation Equation. We assumed that MH does not have mobility, because it is a solid material. Therefore, we defined gas-water two-phase flow in the pore space along with MH formation and dissociation. The flow of gas and water is governed by Darcy's law. The mass conservation equations of gas, water, and MH are expressed by the following equations.

Is phaseis expressed as

$$\nabla \cdot \left(\frac{K k_{rg} \rho_g}{\mu_g} \cdot \nabla \Phi_g \right) + (R_d) + \left(-R_f \right) = \frac{\partial \left(\phi \rho_g S_g \right)}{\partial t}. \quad (1)$$

Water phase is expressed as

$$\nabla \cdot \left(\frac{K k_{rw} \rho_w}{\mu_w} \cdot \nabla \Phi_w \right) + (N_h R_d) + \left(-N_h R_f \right) = \frac{\partial (\phi \rho_w S_w)}{\partial t}. \quad (2)$$

MH derived from irreducible water is expressed as

$$(-R_{d1}) = \frac{\partial (\phi \rho_h S_{h1})}{\partial t}. \quad (3)$$

MH derived from free water is expressed as

$$(-R_{d2}) + \left(+R_f \right) = \frac{\partial (\phi \rho_h S_{h2})}{\partial t}. \quad (4)$$

Here, we have R_d: total dissociation rate of MH, R_{d1}: dissociation rate of MH derived from irreducible water, and R_{d2}: dissociation rate of MH derived from free water. Other symbols are defined in the SYMBOL table. The dissociation rates are related by the following equation:

$$R_d = R_{d1} + R_{d2}. \quad (5)$$

3.2.2. Energy Conservation Equation. Energy is transferred by convection and conduction. MH formation latent heat was assumed to be the same value as that in the dissociation process and of opposite sign:

$$\nabla \cdot \left(\frac{K k_{rg} h_g \rho_g}{\mu_g} \cdot \nabla \Phi_g \right) + \nabla \cdot \left(\frac{K k_{rw} h_w \rho_w}{\mu_w} \cdot \nabla \Phi_w \right) + \nabla \cdot (\lambda_c \cdot \nabla T) + (-H_d R_d) + \left(H_d R_f \right) = \frac{\partial \left(\phi \rho_g S_g U_g + \phi \rho_h S_h U_h + \phi \rho_w S_w U_w + U_r \right)}{\partial t}. \quad (6)$$

3.2.3. Equation of State. Simple equations of state (linear functions) were used to relate the density, enthalpy, and viscosities of the methane and water. The volume fractions (saturations) of all liquid and gas phases and hydrate fraction add to unity:

$$S_g + S_h + S_w = 1. \quad (7)$$

The total MH saturation S_h is expressed as follows:

$$S_h = S_{h1} + S_{h2}. \quad (8)$$

The basic variables in this model are flow potential: Φ_g, Φ_w, saturation of each phase: S_g, S_w, S_{h1}, S_{h2}, and temperature T.

3.3. Formulation for Permeability with MH Formation. It is impossible to experimentally estimate the effect of MH derived from free water on permeability changes. Therefore, we obtained a series of parameters for MH derived from irreducible water experimentally and extended the permeability equations as a function of MH (fraction) to a two-component system. The procedures of formulation permeability have already been described in our previous papers [17, 18].

3.3.1. Absolute Permeability K. We firstly measured water effective permeability K_w under pressure and temperature conditions in which MH has formed from residual water and gas saturations. Three types of sand columns (Toyoura sand, No.7 silica sand, and No.8 silica sand) were used for measurement of K_w. In this study, we assumed that relative permeability to water k_{rw} under the residual gas saturation condition was constant and independent of MH saturation. Therefore, it is possible to estimate K with MH formation by dividing the measured K_w by k_{rw} as follows:

$$K = \frac{K_w}{k_{rw}}. \quad (9)$$

We obtained the result that the relative permeability in the case of an MH saturation of 0.4 was 0.03 compared with the original values without any MH present. This tendency was common and independent of kinds of used sand. Based on the experimental results, we formulated the absolute permeability K as a function of MH fraction, S_{h1}. We selected the equation proposed by Masuda et al. [12]. In

(10), the parameters N_1 (called the reduction factor) and K (permeability) are functions of S_{h1}, the irreducible hydrate fraction. K_0 is the original permeability value of sand column without any MH formation:

$$K = K_0 \cdot (1 - S_{h1})^{N_1}, \tag{10}$$

$$N_1 = 10.384 \cdot {S_{h1}}^2 - 27.773 \cdot S_{h1} + 13.639. \tag{11}$$

The absolute permeability K in the MH two-component system is expressed as follows. In this model, setting the reduction factor N_2 for S_{h2} to be smaller value than N_1 for S_{h1}, it is possible to reproduce the extreme permeability reduction observed in the experiments:

$$K = K_0 \cdot (1 - S_h)^{N_1} \quad (S_h \le S_{h1\max}),$$

$$K = K_0 \cdot (1 - S_{h1\max})^{N_1} \cdot \left(\frac{1 - S_h}{1 - S_{h1\max}}\right)^{N_2} \quad (S_h > S_{h1\max}). \tag{12}$$

Figure 5 shows the dependence of MH saturation on absolute permeability. The value of K at maximamal value $S_{h1\max}$ of S_{h1} decreases significantly as S_{h2} becomes higher as shown in this figure. Furthermore, when whole pore space is occupied by MH ($S_{h1} + S_{h2} = S_h = 1$), K takes on the limiting value of 0.

The change in absolute permeability K from porosity change due to consolidation was considered. As previously mentioned, we found that effective stress was more important that than MH of dissociation when investigating consolidation. Therefore the effect of porosity reduction due to consolidation on permeability change could be independently estimated. The effect of porosity changes on permeability was expressed as a function of the ratio to initial porosity (ϕ/ϕ_0), (13). By combining this equation with (12), we obtained (14) as

$$K_0' = K_0 \cdot \left(\frac{\phi}{\phi_0}\right)^{N_\phi}, \tag{13}$$

$$K = K_0 \cdot \left(\frac{\phi}{\phi_0}\right)^{N_\phi} \cdot (1 - S_{h1\max})^{N_1} \cdot \left(\frac{1 - S_h}{1 - S_{h1\max}}\right)^{N_2}. \tag{14}$$

We used the same apparatus that was used for depressurization experiments and obtained the change in permeability as a function of the porosity ratio (ϕ/ϕ_0) experimentally by conducting consolidation-permeability tests with water that was injected into water-saturated samples. Figure 6 showed the dependence of effective stress on change in axial displacement and change of differential pressure with time during consolidation-permeability test in the case of No.8 silica sand. In this experiment, the rate of axial loading was set to a constant value of 0.141 MPa/min. Differential pressure was gradually increased from 0.500 kPa to 1.90 kPa with time depending on reduction of porosity. Increase in differential pressure indicated a reduction of permeability in the pore space. By changing the initial porosity and sand

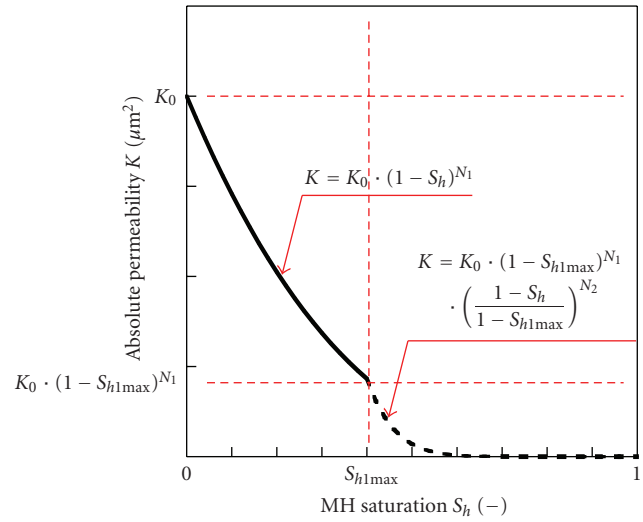

Figure 5: Formulation of absolute permeability as function of MH saturation in MH two-component system.

types, we obtained data which included differential pressure and deformation behavior due to consolidation with time.

The reduction factor N_ϕ in (14) was estimated numerical model calibration. The numerical simulator COTHMA (Coupled thermo-hydro-mechanical analysis with dissociation and formation of methane hydrate in deformation of multiphase porous media), developed by the West Japan Engineering Consultants, Inc., under MH21 Research Consortium, was used. We estimated the increment of displacement and pore pressure for each node in the numerical grid by using the stress-strain relationship obtained in consolidation-permeability tests. In addition, history matching using differential pressure data due to consolidation was carried out by varying the reduction factor N_ϕ. The solid line and dashed one in Figure 6 show the results for the calculation. From this figure, calculation results could reproduce the changes of axial displacement and differential pressure . We only varied the reduction factor N_ϕ in numerical analysis, so this value represents permeability change due to consolidation. For all the simulations, the values of N_ϕ changed from 4.80 to 10.0. We observed the following trends for N_ϕ: (1) N_ϕ became small in the case of large sand grain diameters. (2) N_ϕ became larger in the case of large initial porosity. Therefore, in this study, N_ϕ was formulated as a function of sand grain diameter D_A and initial porosity ϕ_0. The derived equation for N_ϕ is expressed as follows. As basic condition for formulation, we treated sand grain diameter D_{AT}: 200 μm, initial porosity ϕ_{T0}: 0.412, and reduction factor $N_{\phi T}$: 5.50 in the case of Toyoura sand as

$$N_\phi = a_\phi \cdot \left(\frac{D_A}{D_{AT}} - 1\right) + c_\phi \cdot \left(\frac{\phi_0}{\phi_{T0}}\right) + d_\phi. \tag{15}$$

Here, $a_\phi = -3.96$, $c_\phi = 8.55$, and $d_\phi = -2.86$. By introducing (15) into (14), it is possible to consider absolute permeability changes not only from MH dissociation but also from porosity changes due to consolidation.

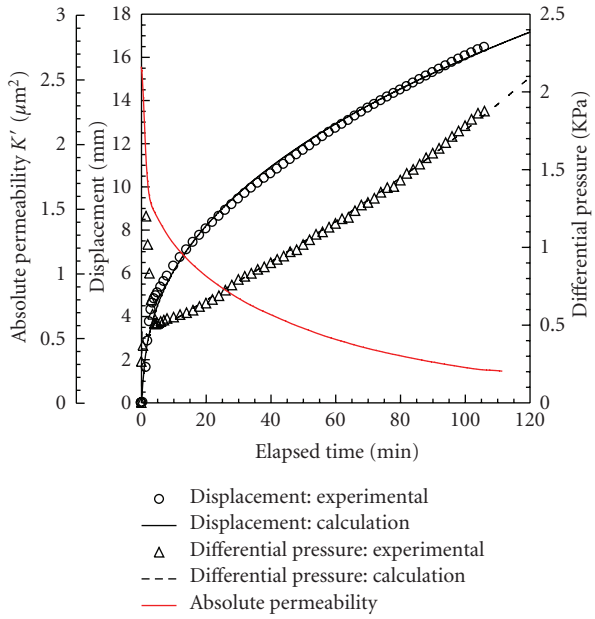

FIGURE 6: Dependence of effective stress on change of axial displacement and change of differential pressure with time during consolidation-permeability test.

3.4. Irreducible Water Saturation S_{wi} and Residual Gas Saturation S_{gr}. Irreducible water saturation S_{wi} and residual gas saturation S_{gr} are very important parameters in order to define the active saturation interval in gas-water multiphase flow for the relative permeability curves used in predicting the amount of dissociated gas. We assumed that the distribution of sand grain constituting real MH sediments is wide ranging and reservoir temperature changes with time due to MH dissociation and hot-water injection. Therefore it is important to estimate the effect of these parameters on flow behavior quantitatively in addition to MH saturation. In this study, we formulated S_{wi} and S_{gr} on the basis of the experimental results of the displacement of free methane gas by cold-water injection.

First of all, we used three types of sand, Toyoura sand, No.7 silica sand, and No.8 silica sand, and considered the effect of average sand grain diameter on changes of S_{wi00}, the average residual water saturation, and S_{gr00}, the average residual gas saturation, without any MH formation. S_{wi00} and S_{gr00} are formulated as functions of D_A/D_{AT}, on the basis of S_{wiT} and S_{grT} of Toyoura measured without any MH formation at 4°C as follows:

$$S_{wi00} = S_{wiT} + (1. - S_{wiT}) \cdot \left(1. - \frac{D_A}{D_{AT}}\right)^{Nw},$$
$$S_{gr00} = S_{grT} \cdot \left(\frac{D_A}{D_{AT}}\right)^{Ng}. \tag{16}$$

Then, S_{wi0} and S_{gr0} were formulated as a function of MH saturations S_{h1} and S_{h2}, in order to extend (16) to account for the presence of MH. It was experimentally observed that if the injection of methane gas was continued after MH formation, then additional water was not observed. Therefore, the difference between the amount of irreducible water under the initial condition and the consumption of water for MH formation corresponds to the amount of irreducible water with MH formation. Figure 7(a) shows the changes in S_{wi0} as functions of MH saturation S_{h1} derived from irreducible water. As S_{h1} increased, S_{wi0} decreased markedly. S_{wi0} changed from 0.324 to 0.116 with MH saturation. S_{wi0} is expressed as a function of only S_{h1}, using S_{wi00} previously formulated as (17) and the volume ratio R_{Vhw} of MH to water:

$$S_{wi0} = S_{wi00} - R_{vhw} S_{h1}. \tag{17}$$

On the other hand, S_{gr} ranged from 0.350 to 0.119 and showed a tendency to decrease with increasing MH saturation as shown in Figure 7(b). S_{gr0} is a function of S_{h1}, S_{h2}, and R_{Vhw}. When all of the pore space was filled with MH, S_{gr0} should become zero. These behaviors are represented by (18):

$$S_{gr0} = S_{gr00} \cdot (1 - S_{h1})^{Nsgr1} \cdot \left[\frac{1 - S_{wi00} - (1 - R_{Vhw}) \cdot S_{h1} - S_{h2}}{1 - S_{wi00} - (1 - R_{Vhw}) \cdot S_{h1}}\right]^{Nsgr2}. \tag{18}$$

Finally, we obtained the following final form of equations for S_{wi} and S_{gr} by extending (17) and (18) as a function of temperature T:

$$S_{wi} = S_{wi0} \cdot \left[a_{swi} \cdot (T - T_0)^2 + b_{swi} \cdot (T - T_0) + c_{swi}\right]^{D_A/D_{AT}},$$
$$S_{gr} = S_{gr0} \cdot \left[a_{sgr} \cdot (T - T_0)^2 + b_{sgr} \cdot (T - T_0) + c_{sgr}\right]^{D_A/D_{AT}}. \tag{19}$$

3.5. Relative Permeabilities k_{rg}, k_{rw}. Using parameters for gas-water multiphase flow, such as S_{wi} and S_{gr}, we formulated the gas and water relative permeabilities k_{rg} and k_{rw}, respectively, when MH is present. In our numerical model, we extended the interval of water saturation S_w in the gas-water multiphase flow with the normalized water saturation S_w^*. Using S_w^*, we were able to use one set of relative permeability curves for any MH saturation condition:

$$S_w^* = \frac{S_w - S_{wi}}{1 - S_{gr} - S_{wi} - (S_{h1} + S_{h2})} = \frac{S_w - S_{wi}}{1 - S_{gr} - S_{wi} - S_h}. \tag{20}$$

The Corey model that is used as a general relative permeability curve is expressed as follows. Here, a and b are the values of k_{rg} and k_{rw} at endpoints on the relative permeability curves. The endpoints are defined as the saturation conditions of S_{wi} and S_{gr}. In addition, the limitations that (1) k_{rg} was set to 1 in the case of $S_w = 0$ and (2) k_{rw} was set to 1 in the case of $S_g = 0$ were adapted in this relative permeability model. The gas and liquid relative permeabilities are shown in (21):

$$k_{rg} = a \cdot (1 - S_w^*)^2 \left[1 - (S_w^*)^2\right],$$
$$k_{rw} = b \cdot (S_w^*)^4. \tag{21}$$

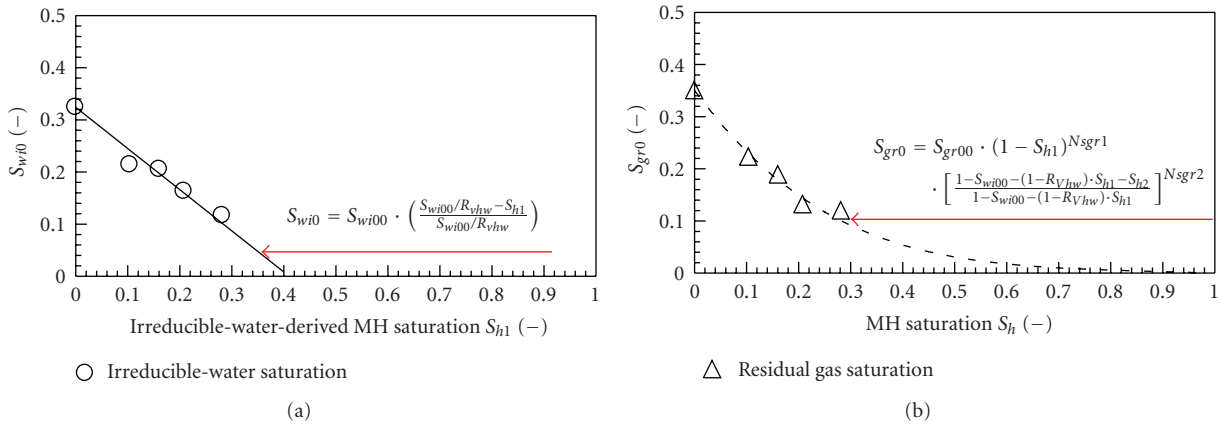

Figure 7: Formulation of irreducible-water saturation and residual gas saturation as functions of MH saturation in MH two-component system.

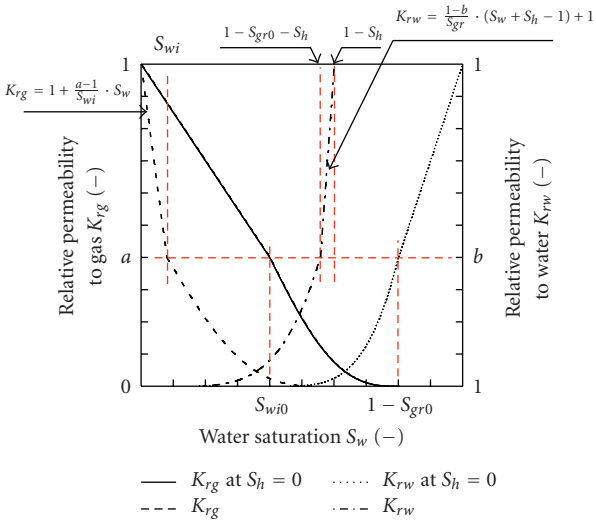

Figure 8: Relative permeability curves for different MH saturation conditions.

Figure 8 shows relative permeability curves for different MH saturation conditions. Both k_{rg} and k_{rw} changed with water saturation S_w and MH saturation S_h as shown in the figure. As MH saturation became higher, the curves were shifted to lower-water-saturation conditions.

4. Numerical Simulation of Laboratory-Scale Experiments for MH Dissociation Process in a Porous Media and Optimization of Permeability Parameters with MH Formation

To validate the numerical model and the developed permeability relationships with MH formation, we carried out numerical simulations of some of the previously mentioned laboratory-scale experiments for MH dissociation by hot-water injection and depressurization and compared the simulation results with experimental results. In this study, the simulation code FEHM (Finite Element Heat and Mass Transfer), developed at the Los Alamos National Laboratory, was used for calculations [19, 20]. In the FEHM code, the conservation equations of energy and mass in a porous media are solved using the control volume finite element method. This code has some advantages for the multicomponent multiphase analysis and phase transformation analysis of MH formation and many permeability models. Originally, this code was developed for the analysis of the geothermal reservoirs. Using the model for MH dissociation process in a porous media as previously mentioned, we modified the FEHM code to include a one-component MH dissociation and formation, a two-component MH dissociation and formation, and a three-phase three-component system that represents gas, water, and MH [21].

4.1. Hot-Water Injection. In numerical simulation for hot-water injection process, we verified the validity of MH two-component model constructed in this study. Figure 9 shows a comparison of the experimental and calculation results for change in differential pressure and gas production behavior during MH dissociation by hot-water injection after extending the MH phase into two components in the simulator. "Two components" in the explanatory note shows the results in the case of MH two-component model developed in this study. For comparison, the results in MH one-component model are also shown in the same figure. "One component: No growth" is the case that MH growth (or MH formation) was not considered. MH growth was considered in the case of "One component: Growth." The change in differential pressure observed in the experiment consists of the following three stages: (1) an increase dependent on viscosity difference between gas and water, (2) a large increase as a result of MH formation in the downstream zone in the sand column, and (3) a permeability decrease as a result of MH dissociation. By introducing MH two-component model into the simulator, the calculation results sufficiently agreed with the experimental results. In regards to gas production behavior, the calculation also reproduced the series of behaviors observed in the experiment that

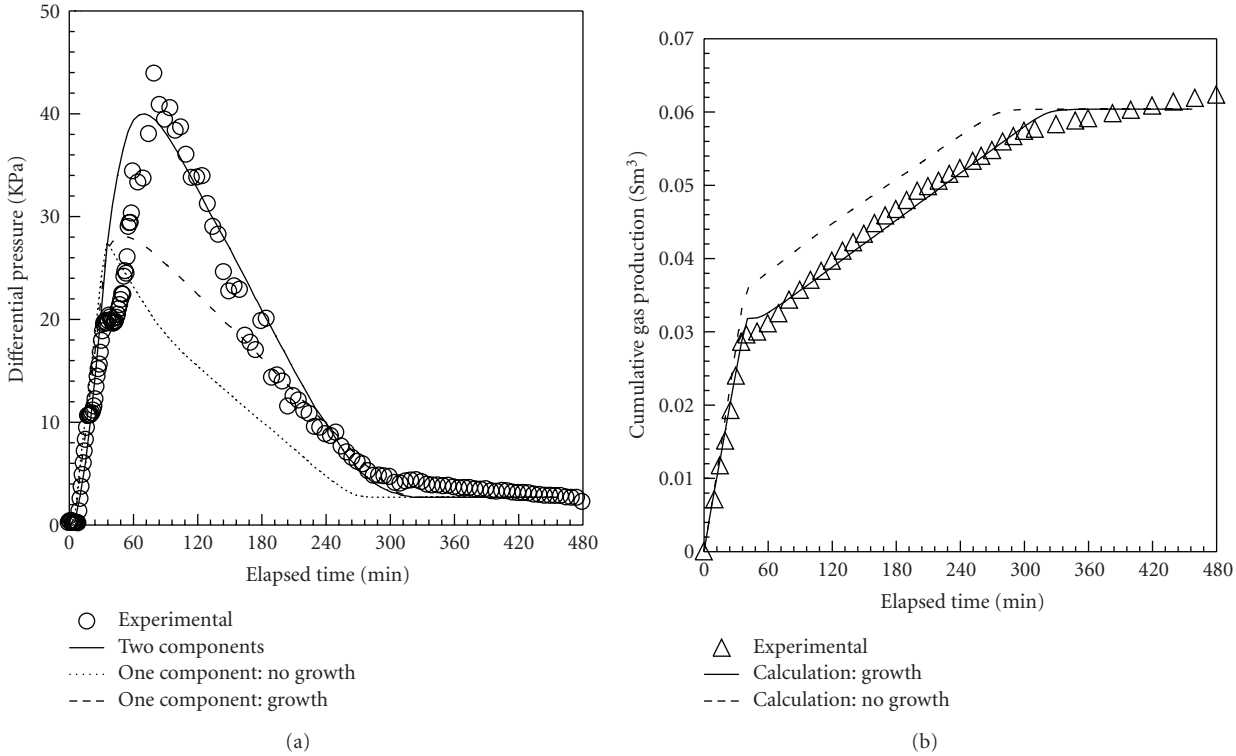

Figure 9: Comparison of experimental and calculation results for change in differential pressure and gas production behavior during MH dissociation by hot-water injection after extending the MH phase into two components.

consisted of (1) displacement of free methane gas, (2) delay of gas production due to MH growth, and (3) dissociated gas production. By comparing simulation and experimental results, it was found that the numerical simulator was able to reproduce temperature change, permeability characteristics, and gas production behavior, associated with both MH formation and dissociation.

4.2. Depressurization. MH dissociation that occurs in depressurization is strongly affected by two thermal processes: (1) latent heat release of MH in sediments and (2) thermal conduction from the surrounding area [22]. In addition, water saturation in pore space at the initial stage is relatively high. As a result, production behavior is accompanied by water displacement induced gas expansion from the pressure decrease and dissociated gas flow. Therefore thermal conductivity and relative permeability in gas-water multiphase flow system are dominant factors on MH dissociation and production behavior. Capillary pressure under the existence of MH is not well known, so we treat the pressure of each phase as identical system pressure in our numerical model. In this study, considering the difference of mobility between gas and water, we tried to reproduce production behavior observed in experiments by optimizing the shape of relative permeability curves. Changes in irreducible water saturation and residual gas saturation due to difference of sand grain size and dissociation are reflected in the relative permeability by the use of the normalized water saturation, (20). Here, as an example of numerical simulation, we present the results of history matching in the case of No.8 silica sand (average sand grain diameter: 115 μm).

As previously mentioned, MH dissociation after a pressure decrease reaches an equilibrium condition limited by thermal conduction from surrounding material. Therefore, preliminary to the consideration of gas-water flow, we carried out history matching of the temperature change in sand column by varying the thermal conductivity of sediment. Yamamoto et al. [23, 24] considered the thermal conductivity λc of sedimentary layers containing MH using the mixture sample of sand and MH. As a result, they observed that λc ranged from about 0.40 to 2.00 W/(m·K) depending on the amount of MH and saturation condition of gas and water. This value depended strongly on the types of sedimentary structure that were formed by the sand and MH. The final result of the formulation for λc has not yet been reported. Therefore, we varied λc within the reported values and estimated the value of λc by comparison with temperature change in the experiments. Figure 10 shows the calculation results for temperature change during the MH dissociation by depressurization. It is generally known that thermal conductivity becomes smaller when gas instead of water fills the pore space. In the calculations, when λc was set to 1.06 W/(m·K), it was found that the change in the temperature distribution was such that (1) a temperature decrease from initial temperature of 11.7°C to an equilibrium condition of 1.70°C was observed with

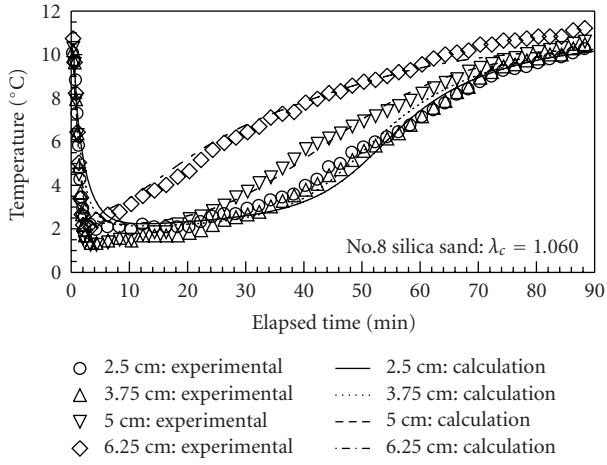

FIGURE 10: Comparison of experimental and calculation results for temperature change with time during MH dissociation by depressurization (No.8 silica sand).

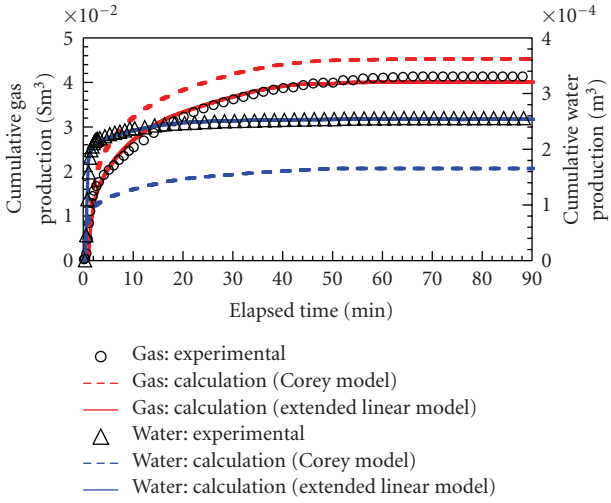

FIGURE 11: Comparison of experimental and calculated results for cumulative productions of gas and water when the different relative permeability curves were used (No.8 silica sand).

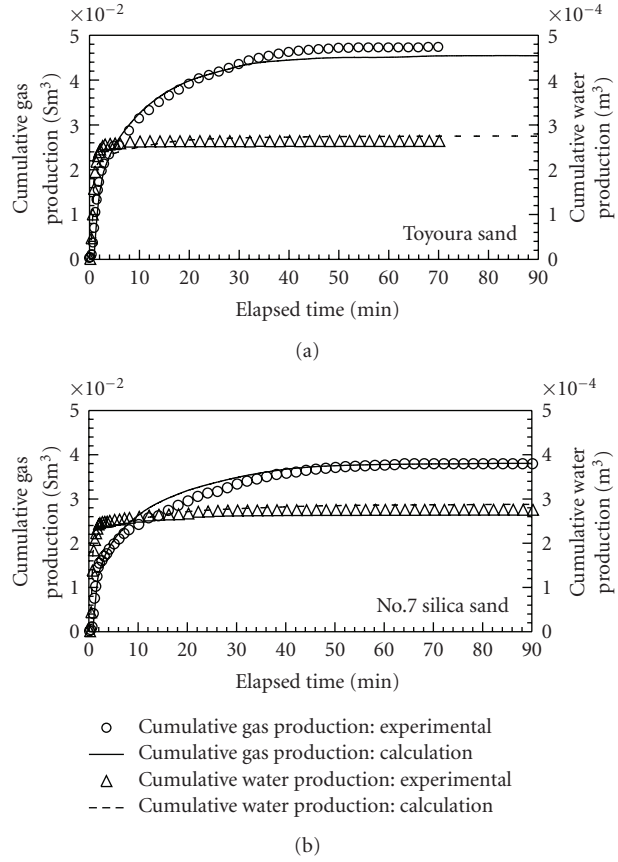

FIGURE 12: Comparison of experimental and calculation results for production behaviors of gas and water in the cases of Toyoura sand and No.7 silica sand.

depressurization, and (2) a temperature increase to the outer boundary temperature after completion of dissociation could be sufficiently reproduced.

Then, we calibrated the gas-water relative permeability curves with MH present through history matching of production behavior during MH dissociation by depressurization. In these experiments, the permeability is relatively high even if solid MH exists in the pore space. Additionally, the effect of consolidation on the gas production behavior was not very large. Therefore, it is assumed that the most dominant parameter on the production behavior is relative permeability. We carried out history matching by using the Corey model expressed as in (21). Figure 11 shows the comparison of the experimental and calculated results for cumulative productions of gas and water when the Corey model was used for the relative permeability curves. From this figure, rapid water discharge at the initial stage and dissociated gas production were similar to the experimental results. However, calculation underestimated the amount of water production (1.8×10^{-4} m^3) whereas the experimentally measured value was 2.55×10^{-4} m^3. On the other hand, the cumulative gas production was estimated as 4.52×10^{-2} Sm^3, so the calculation result overestimated the amount of gas production by approximately 10% compared with the experimental one (4.05×10^{-2} Sm^3). In other words, the estimated amount of gas remaining in the pore space decreased because the water production was underestimated. The reason for the difference between the experiment and calculation is as follows. In the calculation, the pressure of the gas phase is equal to that of the water phase without considering the effect of the capillary pressure. When the Corey model was used for the relative permeability curves, it was impossible to reproduce the observed phenomena in the experiments wherein water was selectively drained under an initial high water saturation condition, and dissociated gas was maintained in the pore space. Therefore, considering the effect of capillary pressure, we optimized the shape of the relative permeability curves so as to yield a water mobility higher than that of gas under the high water saturation condition. For optimization purposes, we introduced the

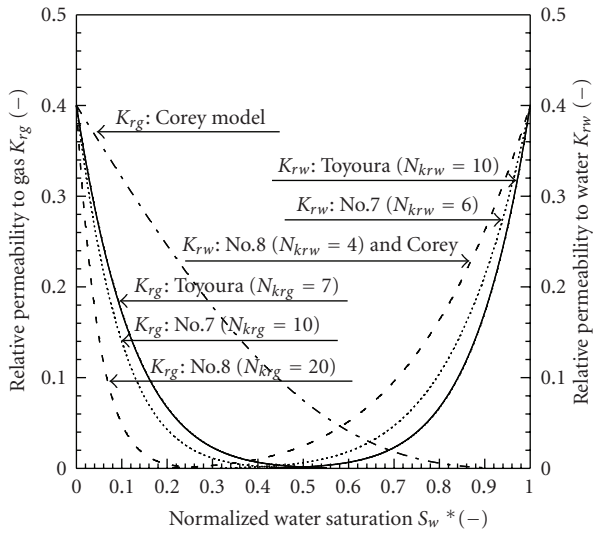

FIGURE 13: Optimized relative permeability curves through series of numerical analysis.

indexes of N_{krg} and N_{krw} into the linear relative permeability model as follows:

$$k_{rg} = a \cdot \left(1 - S_w^*\right)^{N_{krg}}, \tag{22}$$

$$k_{rw} = b \cdot S_w^{*N_{krw}}. \tag{23}$$

When N_{krg} is set to a larger value in (22), the water mobility becomes relatively larger than that of gas. On the other hand, the water mobility became smaller under the condition of larger N_{krw} value. In addition, when N_{krw} is set to 4, k_{rw} is same as that of the Corey model. At $N_{krg} = 2.5$, k_{rg} overlaps with that of the Corey model. Considering the lower relative permeability to gas in the higher water saturation condition, we set N_{krg} and N_{krw} to 20 and 4, respectively. The calculations with these parameters (called extended linear model) are also shown in Figure 11. From this figure, it was found that the calculation could sufficiently reproduce production behavior observed in the experiments containing rapid water production at the initial stage.

Using a similar numerical approach, we conducted history matching of the production behaviors for the cases of Toyoura sand (average sand grain diameter: 200 μm) and No.7 silica sand (average sand grain diameter: 180 μm) as shown in Figure 12. There was excellent agreement between the experimental and simulation results. We used 1.20 W/(m·K) (Toyoura) and 1.90 W/(m·K) (No.7) as the values of thermal conductivity λc. In addition, the reduction factors N_{krg} and N_{krw} for the relative permeability curves were set at 7 and 10 (Toyoura) and 10 and 6 (No.7), respectively, to reproduce the production behavior during the MH dissociation by depressurization. Calibrated relative permeability curves obtained through the simulations are shown in Figure 13. Several trends are apparent. As the sand grain diameter became larger, the gas mobility increased under higher water saturation conditions. This indicates that the effect of capillary pressure decreased owing to the increase in the pore diameter. In addition, the shapes of the relative permeability curves reflect the behaviors observed in our experiments, that is, the amount of water production was not so different despite the decrease in the residual water saturation, S_{wi0}, in the case of larger sand grain diameter.

The simulations also confirmed the validity of formulation of irreducible water saturation S_{wi} and residual gas saturation S_{gr}, expressed as in (16) to (20), and obtained the optimized shape of relative permeability curves to reproduce production behavior during MH dissociation by depressurization.

5. Conclusions

We conducted an experimental study of the MH dissociation process by hot-water injection and depressurization and studied the effect of temperature and permeability changes on gas production. On the basis of experimental results, a numerical model for MH dissociation process in porous media was constructed. In addition, we carried out numerical simulations on laboratory-scale experiments for MH dissociation and verified the validity of the numerical model. Conclusions are summarized as follows.

(1) It was found that MH dissociation by hot-water injection consisted of 4 stages: displacement of free methane gas due to water injection, permeability reduction due to additional MH formation in the downstream zone, actual MH dissociation, and completion of dissociation. MH reformation and growth observed at early times had large effect on dissociation behavior and permeability characteristics.

(2) The decrease of the solid material itself due to MH dissociation had only a small effect on consolidation. Therefore, we confirmed that the increase in the effective stress at the initial stage of depressurization rather than MH dissociation was a dominant factor for the consolidation behavior.

(3) On the basis of the experimental results, a numerical model of MH dissociation in a porous media was designed and implemented in a numerical simulator. In our numerical model, we treated the MH phase as a two-component system by modeling the pore space occupied by MH. One component is derived from irreducible water and is formed so as to cover the surface of a sand grain. The other component is defined as MH made of movable free water and formed at the central pore space so as to plug the flow path.

(4) On the basis of experimental measurements, absolute permeability, relative permeability, irreducible water saturation, and residual gas saturation with MH formation were also formulated as a function of MH saturation, porosity and sand grain diameter and introduced into the numerical model.

(5) Using the developed simulator, we attempted history matching for a laboratory-scale experiment for MH dissociation by hot-water injection. It was found that

this simulator developed was able to reproduce temperature change, permeability characteristics, and gas production behavior, associated with both MH formation and dissociation.

(6) Through history matching for temperature change during MH dissociation by depressurization, the effect of thermal conductivity on dissociation behavior was discussed. We obtained calibrated values of the apparent thermal conductivity of sediments containing MH. On the basis of production behavior, we optimized the shape of the relative permeability curves so as to reproduce observed water and gas production at both low and high water saturation conditions. The indexes of N_{krg} and N_{krw} were introduced into the linear relative permeability model in order to consider the effect of capillary pressure. As a result, the numerical simulations could more accurately reproduce production behavior during the depressurization process .

Symbols

a: Coefficient for gas relative permeability
a_{sgr}: Coefficient for calculation of residual gas saturation ($= -3.749E-05$)
a_{swi}: Coefficient for calculation of irreducible water saturation ($= 3.913E-06$)
a_ϕ: Coefficient for calculation of absolute permeability ($= -3.96$)
b: Coefficient for water relative permeability
b_{sgr}: Coefficient for calculation of residual gas saturation ($= 9.764E-03$)
b_{swi}: Coefficient for calculation of irreducible water saturation ($= -3.438E-03$)
c_{sgr}: Coefficient for calculation of residual gas saturation ($= 0.980$)
c_{swi}: Coefficient for calculation of irreducible gas saturation ($= 1.048$)
c_ϕ: Coefficient for calculation of absolute permeability ($= 8.55$)
D_A: Average sand grain diameter, m
D_{AT}: Average sand grain diameter of Toyoura sand, m ($= 2.000E-04$)
$d_{\phi r}$: Coefficient for calculation of absolute permeability ($= -2.86$)
H_d: Heat of dissociation, J/mol
h_g: Enthalpy of gas, J/mol
h_w: Enthalpy of water, J/mol
K: Absolute permeability, m^2
K_0: Absolute permeability without any MH formation, m^2
k_{rg}: Relative permeability to gas
k_{rw}: Relative permeability to water
N_1: Reduction factor for calculation of absolute permeability
N_2: Reduction factor for calculation of absolute permeability
N_g: Reduction factor for calculation of S_{gr00}
N_h: Hydrate number
N_{krg}: Reduction factor for calculation of k_{rg} in linear relative permeability model
N_{krw}: Reduction factor for calculation of k_{rw} in linear relative permeability model
N_{sgr1}: Reduction factor for calculation of S_{gr0}
N_{sgr2}: Reduction factor for calculation of S_{gr0}
N_w: Reduction factor for calculation of S_{wi00}
N_ϕ: Reduction factor for calculation of absolute permeability
$N_{\phi T}$: Reduction factor for calculation of absolute permeability ($= 5.50$)
R_d: Dissociation rate of MH, mol/(m$^3\cdot$s)
R_f: Gas consumption rate due to MH growth, mol/(m$^3\cdot$s)
R_{Vhw}: Volume ratio of MH to water.
S_g: Gas saturation
S_{gr}: Residual gas saturation
S_{gr0}: Residual gas saturation as function of MH saturation
S_{gr00}: Residual gas saturation as function of average sand grain diameter
S_{grT}: Residual gas saturation for Toyoura sand without any MH formation
S_h: MH saturation
S_w: Water saturation
S_{wi}: Irreducible water saturation
S_{wi0}: Irreducible water saturation as function of MH saturation
S_{wi00}: Irreducible water saturation as function of average sand grain diameter
S_{wiT}: Irreducible water saturation for Toyoura sand without any MH formation
S_w^*: Normalized water saturation
T: Temperature, K
T_0: Standard temperature, K ($= 273.15$)
∂t: Time step, sec
U_g: Internal energy of gas, J/mol
U_h: Internal energy of MH, J/mol
U_r: Internal energy of rock, J/m^3
U_w: Internal energy of water, J/mol
μ_g: Gas viscosity, Pa$\cdot$s
μ_w: Water viscosity, Pa$\cdot$s
λ_c: Apparent heat conductivity of reservoir, J/(s$\cdot$K)
ρ_g: Mole weight of gas, mol/m^3
ρ_h: Mole weight of MH, mol/m^3
ρ_w: Mole weight of MH, mol/m^3
Φ_g: Flow potential of gas phase, Pa
Φ_w: Flow potential of water phase, Pa
ϕ: Porosity
ϕ_0: Initial porosity
ϕ_{T0}: Initial porosity for Toyoura sand ($= 0.412$).

Acknowledgments

This work was financially supported by Japan's Methane Hydrate R&D Program (MH21 Research Consortium) planned by Ministry of Economy, Trade and Industry

(METI). The authors thank Mr. T. Ohno, Ms. M. Kakumoto, and Ms. T. Nemoto for conducting the experimental and numerical studies of gas hydrates.

References

[1] Y. F. Makogon, *Hydrates of Natural Gas*, Pennwell, Tulsa, OK, 1981.

[2] Y. F. Makogon, "Natural gas hydrates: the state of study in the USSR and perspectives for its use," in *Proceedings of The 3rd Chemical Congress of North America*, Toronto, Canada, June 1988.

[3] Y. Okuda, "Sherbet-like natural gas resources—gas hydrate," *Petrotech*, vol. 16, pp. 300–305, 1993.

[4] M. Sato and Y. Aoki, "Gas hydrate (IV), geology and prospecting of methane hydrate," *The Japan Institute of Energy*, vol. 80, pp. 973–995, 2001.

[5] M. Sato, "Gas hydrate (III), distribution of methane hydrate, amount of methane, and resources," *The Japan Institute of Energy*, vol. 80, pp. 1064–1074, 2001.

[6] M. Kurihara, K. Funatsu, H. Ouch, Y. Masuda, and H. Narita, "Investigation on applicability of methane hydrate production methods to reservoirs with diverse characteristics," in *Proceedings of the 5th International Conference on Gas Hydrate*, vol. 3, pp. 714–725, Trondheim, Norway, 2005.

[7] A. Masui, H. Haneda, Y. Ogata, and K. Aoki, "Effects of methane hydrate formation on shear strength of synthetic methane hydrate sediments," in *Proceedings of The 15th International Offshore and Polar Engineering Conference Seoul*, pp. 19–24, Korea, June, 2005.

[8] M. H. Yousif, H. H. Abass, M. S. Selim, and E. D. Sloan, "Experimental and theoretical investigation of methane gas hydrate dissociation in porous media," in *Proceedings of the 63rd Annual Technical Conference and Exhibition of the Society of Petroleum Engineers*, pp. 571–583, Houston, Tex, USA, 1988.

[9] M. S. Selim and E. D. Sloan, "Hydrate dissociation in sediment," in *Proceedings of the 62nd Annual Technical Conference and Exhibition of the Society of Petroleum Engineers*, pp. 243–258, Dallas, Tex, USA, 1987.

[10] L. Jeannin, G. Bayi, O. Remard, O. Bonnefoy, and J. M. Herri, "Formation & dissociation of methane hydrate in sediments—part II: numarical modelig modeling," in *Proceedings of the 4th International Conference on Gas Hydrate*, vol. 2, pp. 802–806, Yokohama, Japan, 2002.

[11] G. D. Holder and P. F. Angert, "Simulation gas production from a reservoir containing both gas hydrate and free natural gas," in *Proceedings of the 57th Annual Fall Technical Conference and Exhibition of the Society of Petroleum Engineers of AIME*, New Orleans, Fla, USA, 1982, SPE 11105.

[12] Y. Masuda, M. Kurihara, H. Ohuchi, and T. Sato, "A field-scale simulation study on gas productivity of formations containing gas hydrates," in *Proceedings of the 4th International Conference on Gas Hydrate*, vol. 1, pp. 40–46, Yokohama, Japan, 2002.

[13] Y. Sakamoto, T. Komai, T. Kawamura, H. Minagawa, N. Tenma, and T. Yamaguchi, "Laboratory-scale experiment of methane hydrate dissociation by hot-water injection and numerical analysis for permeability estimation in reservoir—part 1: numerical study for estimation of permeability in methane hydrate reservoir," *International Journal of Offshore and Polar Engineering*, vol. 17, no. 1, pp. 47–56, 2007.

[14] Y. Sakamoto, T. Komai, H. Haneda, T. Kawamura, N. Tenma, and T. Yamaguchi, "Experimental study on modification of permeability in a methane hydrate reservoir and gas production behavior by the simultaneous injection of nitrogen and hot water," in *Proceedings of the 5th International Conference on Gas Hydrate*, vol. 3, pp. 866–874, Trondheim, Norway, 2005.

[15] Y. Sakamoto, T. Komai, Y. Kawabe, and T. Yamaguchi, "Properties of multiphase flow in marine sediments with gas hydrate," in *Proceedings of the 5th ISOPE Ocean Mining Symposium*, pp. 171–175, Tsukuba, Japan, 2003.

[16] Y. Sakamoto, M. Shimokawara, K. Ohga, et al., "Numerical study on dissociation of methane hydrate and gas production behavior in laboratory-scale experiments for depressurization—part 3: numerical study on estimation of permeability in methane hydrate reservoir," *The International Society of Offshore and Polar Engineers*, vol. 19, pp. 124–134, 2009.

[17] Y. Sakamoto, T. Komai, T. Kawamura, H. Minagawa, N. Tenma, and T. Yamaguchi, "Modification of permeability model and history matching of laboratory-scale experiment for dissociation process of methane hydrate—part 2: numerical study for estimation of permeability in methane hydrate reservoir," *International Journal of Offshore and Polar Engineering*, vol. 17, no. 1, pp. 57–66, 2007.

[18] Y. Sakamoto, M. Shimokawara, K. Ohga, et al., "Field scale simulation for consolidation and gas production behavior during depressurization process of methane hydrate in marine sediments," in *Proceedings of Offshore Technology Conference*, Houston, Tex, USA, 2008, OTC19283.

[19] G. Zyvoloski, Z. Dash, and S. Kelkar, "FEHMN 1.0 finite element heat and mass transfer code," Tech. Rep. LA-12062-MS, Rev.1, Los Alamos National Laboratory, Los Alamos, Calif, USA, 1992.

[20] G. Zyvoloski, "FEHM: a control volume finite element code for simulating subsurface multi-phase multi-fluid heat and mass transfer," Tech. Rep. LAUR-07-3359, Los Alamos National Laboratory, Los Alamos, Calif, USA, 2007.

[21] R. J. Pawar, G. A. Zyvoloski, N. Tenma, Y. Sakamoto, and T. Komai, "Numerical simulation of laboratory experiments on methane hydrate dissociation," in *Proceedings of the 15th International Offshore and Polar Engineering Conference*, vol. 1, pp. 379–385, Seoul, South Korea, 2005.

[22] M. Kurihara, A. Sato, H. Ouchi, H. Narita, and Y. Masuda, "Prediction of gas productivity from Eastern Nankai Trough methane-hydrate reservoirs," in *Proceedings of Offshore Technology Conference*, Houston, Tex, USA, 2008, OTC19382.

[23] Y. Yamamoto, T. Kawamura, M. Ohtake, et al., "Measurement of thermal conductivity of artificial hydrate sediment sample," in *Proceedings of the 14th International Offshore and Polar Engineering Conference*, pp. 36–40, Toulon, France, 2004.

[24] Y. Yamamoto, T. Kawamura, M. Ohtake, et al., "Measurement of thermal conductivity of hydrate sediment sample," in *Proceedings of the 15th International Offshore and Polar Engineering Conference*, vol. 1, pp. 341–345, Seoul, South Korea, 2005.

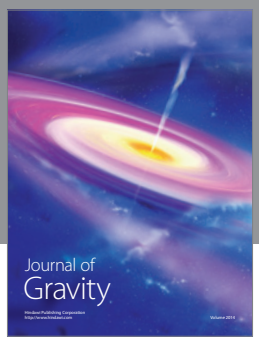

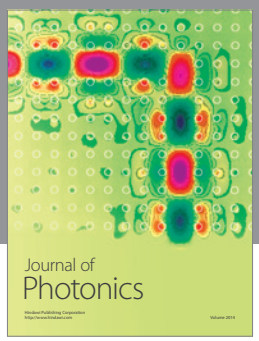

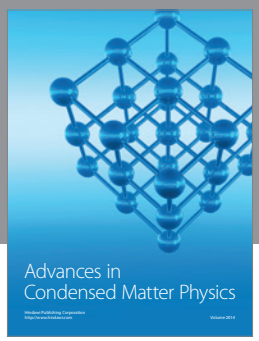

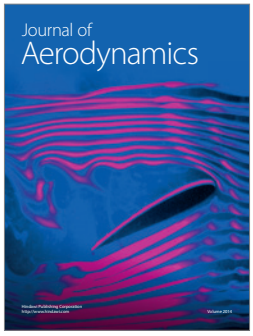

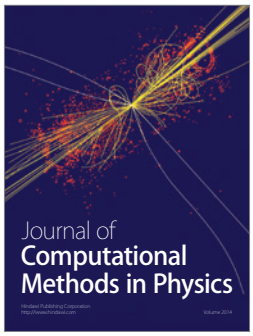

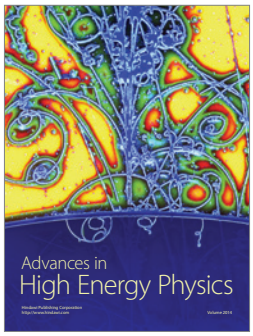

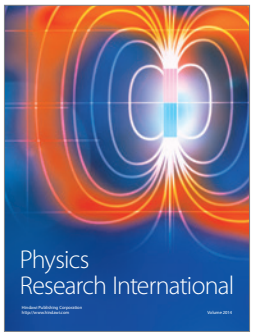

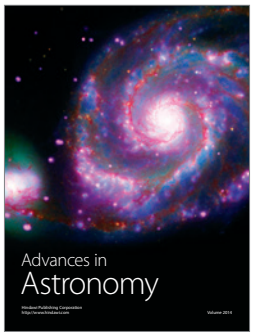

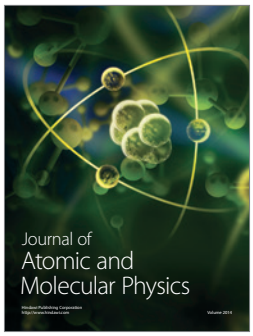

Hindawi

Submit your manuscripts at
http://www.hindawi.com